J. Phys. C: Solid State Phys., **18** (1985) 1377–1386. Printed in Great Britain

# Time evolution of the excess energy in supersaturated solid solutions: microcalorimetric experiments, computer simulations and theory

J Marro†, R Toral† and A M Zahra‡

† Departamento de Física Teórica, Universidad de Barcelona, Diagonal 647, 08028 Barcelona, Spain

‡ CNRS, Centre de Thermodynamique et Microcalorimétrie, 26 Rue de 141é RIA, 13003 Marseille, France

Received 28 March 1984, in final form 2 August 1984

**Abstract.** We describe, compare and analyse a series of microcalorimetric experiments and computer simulations focusing on the temporal behaviour of the excess energy in supersaturated solid solutions, e.g. quenched Al–Zn alloys with different compositions. Both systems, real samples and computer models, show a qualitatively very similar behaviour. The main common features are the scaling of the data corresponding to different compositions, temperatures and even systems, and its consistency with a combination of simple power laws. These facts confirm and extend some previous conclusions about the microscopic mechanisms present during the temporal evolution of the system. We also estimate equilibrium energy values in the case of the binary alloy or Ising model.

## 1. Introduction

The decomposition kinetics of a supersaturated solid solution is a problem of practical as well as theoretical interest. Accordingly it has recently been the subject of many experiments, namely electron or field ion microscopy, electrical resistivity measurements and, most frequently, small-angle scattering of x-rays, light or neutrons (see, for example, Goldburg 1982). The simplest situation of this kind occurs when a segregating binary alloy such as Al–Zn is quenched from the melt into the miscibility gap, a process that can also be simulated on a computer (Binder *et al* 1979, for instance). A recent series of such computer simulations has described the behaviour of the structure function (Lebowitz *et al* 1982, Fratzl *et al* 1983, Marro and Vallés 1983) and the equilibrium shape and evolution of the cluster distribution (Marrow and Toral 1983, Penrose *et al* 1984); they have also revealed a striking and useful similarity between the temporal behaviour of some real materials and that of simple Ising-like models (Lebowitz *et al* 1983).

This paper describes a new effort, from a novel point of view, to understand the mechanisms present during the relaxation of a supersaturated solution. It describes and analyses, probably for the first time, a series of microcalorimetric measurements of the excess energy during the temporal evolution of quenched aluminium alloys. By making a comparison with the behaviour of a simple model system and with some theory we are

0022-3719/85/071377 + 10 $02.25  

able to draw conclusions about the physical mechanisms that seem to dominate during the process. Our results seem more conclusive (although perhaps not so useful) than those obtained when one analyses directly the cluster distribution; this is due in part to the existence of a simple scaling of the data with temperature, composition and even the system investigated.

## 2. The model system

The model, which has been described extensively elsewhere (Marro *et al* 1975, Binder *et al* 1979, Lebowitz *et al* 1983), is a simple cubic lattice with $N = L^3$ ($L = 30$ or 50) lattice sites, each occupied by either an A or a B particle, and periodic boundary conditions. The number of A particles is given by $\rho N$. Starting at a very high temperature (random distribution of the A particles), the system evolves by Kawasaki dynamics, a Markov process whose basic step is to interchange an A particle with a neighbouring B particle with a probability, chosen to satisfy detailed balancing,

$$P(T, \delta U) = \tau_0^{-1} \, \mathrm{e}^{-\beta\delta U}/(1 + \mathrm{e}^{-\beta\delta U}). \tag{1}$$

Here $\beta = 1/k_B T$ and $\delta U$ is the increase of energy brought about by the proposed interchange. The (configurational) energy is defined

$$U = -K \sum_{\mathrm{NN}} s_i s_j \qquad K > 0 \tag{2}$$

where the sum is over nearest-neighbour pairs and $s_i = 1$ $(-1)$ according to whether there is an A (B) particle at site $i$. $\tau_0$, the average time between two attempts to interchange two neighbouring particles, sets the timescale for the evolution; it is taken to be $\tau_0 = 1$ here.

The phase diagram of the corresponding infinite system is accurately known from series expansions. The critical temperature $T_c$ is very close to $4K/0.88686\, k_B$. We shall refer in the following to the system evolution at different values of the density $\rho$ and temperature $T$, $P_{1\text{–}16}$; these are defined in table 1 and in figure 1.

## 3. Equilibrium energy

The energy of the system can also be written as $U = -K(N_{AA} + N_{BB} - N_{AB})$ where $N_{AA}$, $N_{BB}$ and $N_{AB}$ represent, respectively, the number of nearest-neighbour pairs AA, BB and AB in the system; $N_{AA} + N_{BB} + N_{AB} = 3N$. It then follows that

$$U = KN(2u - 3) \tag{3}$$

so that $u \equiv N_{AB}/N$, the number of AB bonds per lattice site, is a natural measure of the system energy.

The computer simulations provided us with values of the energy at selected values of the time, $u_t$, as it evolves towards its asymptotic or equilibrium value $u_\infty(T)$. For comparisons with microcalorimetric measurements on real materials, however, one is rather more interested in the evolution of the *excess energy* $u_t - u_\infty$ at temperature $T$. However, we do not have a definite way of estimating theoretically $u_\infty(T)$ at $T < T_c$ inside the coexistence line. On the other hand, the simulations rarely reach the final equilibrium state in this case and the data are not smooth enough to allow a sensible

evaluation of time derivatives. One may instead assume (Marro *et al* 1975) that the energy of the system with two coexisting phases will be given approximately as a sum of two terms:

$$u_\infty(T) \simeq u^{\mathrm{P}}(T) + \sigma(T)\, u^{\mathrm{I}}(0) \tag{4}$$

where $u^{\mathrm{P}}(T)$ is the equilibrium energy in the pure phase (Baker 1963, Binder 1972). The last term in (4) is intended to represent $u^{\mathrm{I}}(T)$, the contribution of the system interfacial energy at $T < T_c$; $\sigma(T)$ is the surface tension and $u^{\mathrm{I}}(0)$ is the contact surface at zero temperature.

From geometrical arguments it readily follows that

$$u^{\mathrm{I}}(0)\, L = \begin{cases} 6\rho^{2/3} & 0 \leqslant \rho \leqslant \frac{64}{729} \\ 4\rho^{1/2} & \frac{64}{729} \leqslant \rho \leqslant \frac{1}{4} \\ 2 & \frac{1}{4} \leqslant \rho \leqslant \frac{1}{2} \end{cases} \tag{5}$$

in order that the minority phase adopts the minimum contact energy in a system with periodic boundary conditions. Computing $\sigma(T)$ from the Monte Carlo data of Leamy *et al* (1973), we finally obtain the values for $u_\infty$ shown in table 1. In the cases where we were able to obtain estimates of $u_\infty(T)$ from the computer evolution of the model system, these are also shown in table 1 for comparison. One may conclude from the values in

**Table 1.** Definition of the phase points $P_i$, $i = 1, \ldots, 16$, considered in the text and in figure 1. The last column lists the values for the equilibrium energy $u_\infty(T, \rho)$ for the model system as estimated from (4). The values for $u_\infty$ obtained from the computer simulation at $P_1$, $P_8$ and $P_{14}$ (coexistence line) are also shown. These are in perfect agreement with the theoretical predictions. When the model system was quenched to the other phase points, it never reached the equilibrium state; nevertheless, the table also includes for comparison some values of $u_t$ at large enough values of $t$. It seems that our estimates based on equation (4) are good enough at least for $\rho < 0.2$.

| Phase point | | | $u_\infty(T, \rho)$ | |
|---|---|---|---|---|
| $i$ | $\rho$ | $T/T_c$ | Simulation | Theory |
| 1 | 0.01456 | 0.59 | 0.0821 ± 0.0001 | 0.08 |
| 2 | 0.05 | 0.59 | 0.16† | 0.16 ± 0.01 |
| 3 | 0.06 | 0.59 | 0.26† | 0.17 ± 0.02 |
| 4 | 0.075 | 0.59 | 0.19† | 0.18 ± 0.02 |
| 5 | 0.10 | 0.59 | 0.23† | 0.20 ± 0.03 |
| 6 | 0.20 | 0.59 | 0.34† | 0.37 ± 0.05 |
| 7 | 0.50 | 0.59 | 0.42† | 0.4 ± 0.1 |
| 8 | 0.0613 | 0.78 | 0.3072 ± 0.0001 | 0.31 |
| 9 | 0.075 | 0.78 | 0.36† | 0.42 ± 0.05 |
| 10 | 0.10 | 0.78 | 0.45† | 0.51 ± 0.06 |
| 11 | 0.124 | 0.78 | 0.52† | 0.53 ± 0.06 |
| 12 | 0.20 | 0.78 | 0.61† | 0.6 ± 0.1 |
| 13 | 0.50 | 0.78 | 0.72† | 0.65 ± 0.10 |
| 14 | 0.124632 | 0.89 | 0.5458 ± 0.0002 | 0.55 |
| 15 | 0.20 | 0.89 | 0.72† | 0.73 ± 0.10 |
| 16 | 0.50 | 0.89 | 0.82† | 0.75 ± 0.15 |

† At the final time during the evolution.

table 1 that the approximation (4) and our theoretical estimates for $u_\infty(T)$ are good enough at low densities, say $\rho < 0.2$.

## 4. Microcalorimetric measurements

The following binary Al–Zn alloys were analysed at $T \simeq 0.59\,T_c$: Al–5.3 at.% (11.9 wt%)Zn, 6.8 at.% (15 wt%), 9.9 at.% (21 wt%) and 12.1 at.% (25 wt%). The corresponding phase points are denoted by $P_{17\text{–}20}$ respectively; see figure 1. In addition, the Al–6.8 at.% (15 wt%)Zn alloy was also analysed at $0.64\,T_c$; this is referred to as $P_{21}$. Note that the coexistence line corresponding to Al–Zn does not have the symmetry properties characteristic of the model in § 2 (see figure 1); as a consequence, one should not make a direct comparison between the phase points in the group $P_{1\text{–}16}$ and the ones at the same density in the group $P_{17\text{–}21}$.

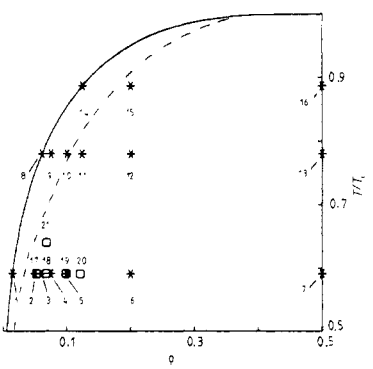


**Figure 1.** Temperature–density section of the phase diagram. The full curve is the coexistence curve corresponding to the model system described in § 2. The broken curve is the estimated coexistence line corresponding to the Al–Zn alloy (Murray 1983). We report equilibrium values and the temporal evolution of the energy in the case of a computer model quenched to the phase points $P_i$, $i = 1, \ldots, 16$ (stars) and in the case of a real Al–Zn alloy quenched to $P_i$, $i = 17, \ldots, 21$ (circles).

The samples were kindly supplied to us by Cégédur–Péchiney, France; the maximal impurity contents are 0.004 wt% Cu, 0.003%Fe and 0.003%Si. Several different temperatures in the single-phase region were used: 275, 400 and 525 °C. After homogenisation for at least 2 h, the solid solutions were transferred into a differential microcalorimeter of the Tian–Calvet type stabilised at temperature between 30 and 170 °C. The estimated cooling rate in these air-cooled samples was about 30 °C $\text{min}^{-1}$, and hence was far from ideal. The exothermal heat effects, $-\mathrm{d}H/\mathrm{d}t$, which accompany the isothermal decomposition of the supersaturated solid solutions, were recorded as a function of the time as long as there was a measurable heat output (in general over ten days). By integrating these heat effects backwards from infinite time, the enthalpy still stored in the decomposing solid solutions may be evaluated at any time except at the very beginning (say < 30 min) of the process when the microcalorimeter is far from thermal

equilibrium owing to the introduction of the samples. The enthalpy we measure

$$-(H_\infty - H_t) = -\int_t^\infty \frac{dH}{dt}\,dt \tag{6}$$

corresponds to the excess energy, $U_t - U_\infty$, present in the alloy at any moment, as the variations of the internal energy of a solid may be related to the enthalpic variations according to $\Delta H = \Delta U + P\Delta V + V\Delta P$. Thus (6) can be compared with $u_t - u_\infty$ via equation (3).

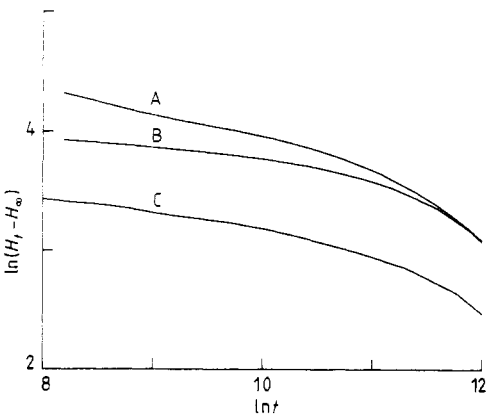


**Figure 2.** Log–log plot of the excess energy versus time (arbitrary units) in the case of the microcalorimetric measurements at $P_{17}$ and $P_{18}$ (curves A and B respectively) and the simulation at $P_5$ (curve C); the temporal behaviours shown at different phase points are all qualitatively very similar.

## 5. Scaling factors

Figure 2 is a logarithmic plot of the excess energy versus time: two microcalorimetric measurements, $P_{17}$ and $P_{18}$, are compared with the results from a computer simulation, $P_5$. The graph suggests that one may introduce scaled variables

$$U^* = \alpha_1 U \qquad t^* = \alpha_2 t \tag{7}$$

in order to stress the similarity between sets of values corresponding to different phase points. Here $\alpha_1$ and $\alpha_2$ are scaling factors such that, in terms of the reduced variables $U^*$ and $t^*$, a set of values corresponding to a given phase point is shifted to overlap the data corresponding to a reference phase point when plotting $\ln(U_t^* - U_\infty^*)$ versus $\ln t^*$. We shall first use $P_5$ ($\rho = 0.10$, $T \simeq 0.6\,T_c$) as the (arbitrary) reference, i.e. $\alpha_1$ and $\alpha_2$ equal unity in the case of $P_5$. Table 2(*a*) lists the values we obtain for $\alpha_1$ and $\alpha_2$ at different densities and temperatures from a least-squares fit in the case of $P_i$, $i = 2$–5, 11, 12, 16–18. An arbitrary example of the scaling one obtains in this way is shown in figure 3 where the data from a real experiment ($P_{18}$) do indeed lie on the curve obtained from the computer simulation at $P_5$.

**Table 2.** (*a*) Values for $\alpha_1$, $\alpha_2$ and $u_\infty$ used to scale the data at the phase points indicated ('shallow quenches'). They were obtained by requiring the best fit to the data at $P_5$ when plotting $\ln(U_i^* - U_\infty^*)$ versus $\ln t^*$; see equation (7). (*b*) As (*a*), in the case of 'deep quenches', with reference to the phase point $P_6$. The values for $P_6$, however, were chosen to produce the best fit to the data at $P_5$ (see figure 4).

| $i$ | $1/\alpha_2$ | $1/\alpha_1$ | $u_\infty(T, \rho)$ |
|---|---|---|---|
| (*a*) | | | |
| 2 | 4.5 ± 0.2 | 0.45 ± 0.02 | 0.157 |
| 3 | 3.7 ± 0.1 | 0.51 ± 0.02 | 0.18 |
| 4 | 1.75 ± 0.05 | 0.75 ± 0.05 | 0.191 |
| 5 | 1 | 1 | 0.23 |
| 11 | 0.024 ± 0.004 | 0.32 ± 0.03 | 0.52 |
| 12 | 0.15 ± 0.02 | 0.80 ± 0.05 | 0.61 |
| 16 | 4.5 ± 0.2 | 1.5 ± 0.2 | 0.71 |
| 17 | (155 ± 5)s | (270 ± 10) J/mol | — |
| 18 | (120 ± 5)s | (330 ± 10) J/mol | — |
| (*b*) | | | |
| 6 | 0.385 | 1.765 | 0.34 |
| 7 | 0.73 ± 0.04 | 2.5 ± 0.2 | 0.38 |
| 13 | 0.46 ± 0.04 | 2.1 ± 0.2 | 0.64 |
| 19 | (40 ± 2)s | (490 ± 20) J/mol | — |
| 20 | (9.2 ± 0.8)s | (215 ± 15) J/mol | — |

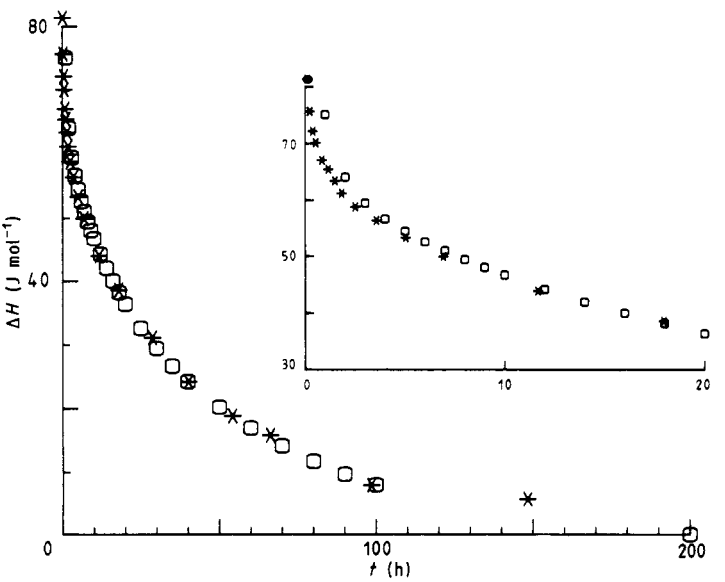


**Figure 3.** The excess energy is plotted here versus time. The stars correspond to $P_5$ (simulation data with arbitrary units), the circles correspond to $P_{18}$ (Al–Zn alloy) using $\alpha_1^{-1} = 330$ J mol$^{-1}$ and $\alpha_2^{-1} = 120$ s; these values seem to have the expected order of magnitude (see the text).

The scaling factors used for figure 3 are respectively $\alpha_1^{-1} = 330\ \mathrm{J\,mol^{-1}}$ and $\alpha_2^{-1} = 120\ \mathrm{s}$, as shown by table 2(*a*). Interestingly these values have the expected order of magnitude. As a matter of fact, taking the Essam and Fisher (1963) value for $K/k_B T_c$ it readily follows from (3) that

$$\alpha_1^{-1} = 2KN_0 = 0.44343\, N_0 k_B T_c \tag{8}$$

where $N_0$ is Avogadro's number. Assuming that the critical temperature for the Al–Zn alloy is 597 K (Schwahn and Schwatz 1978) we have roughly $\alpha_1^{-1} \simeq 2200\ \mathrm{J\,mol^{-1}}$. Concerning $\alpha_2$, we note that (1) indicates the interpretation of $(2\tau_0)^{-1}$ as the rate probability when no change of energy is produced; using the Einstein relation for the diffusivity, $D = (a_0^2/2\tau_0)/6$, where $a_0$ is the lattice spacing, one has

$$\alpha_2^{-1} = a_0^2/12D \tag{9}$$

from which follows the crude estimate $\alpha_2^{-1} \simeq 110\ \mathrm{s}$ at $T = 0.6\ T_c$.

The above estimates for $\alpha_1$ and $\alpha_2$ are admittedly crude. For instance, we have neglected the expected dependence of the scaling factors on the density $\rho$: larger densities cause a faster evolution of the system during the simulation (thus requiring larger values for $\alpha_2$) and larger values of the energy (thus decreasing $\alpha_1$). This behaviour is qualitatively evident in table 2(*a*). In spite of this and other oversimplifications, it is remarkable that the values in table 2(*a*) seem to have the expected order of magnitude. In fact, the observed differences may be interpreted as consequences of the model's simplicity: simple cubic lattice versus the FCC lattice with defects and lattice strains in the case of a real Al–Zn alloy, a sudden quench versus the slow process described in § 4, important differences when one compares the two coexistence curves (figure 1), etc. We firmly believe this is another manifestation of the striking similarity between the behaviour of real systems and computer models (intimately related to a kind of 'universality') that one observes near a phase transition even when kinetic processes are involved (see also Lebowitz *et al* 1983, for instance).

When preparing table 2(*a*) we found it *impossible* to 'normalise' the behaviour at, say $P_7$ or $P_{13}$ to that at $P_5$. Instead it seems that $P_6$ (or $P_7$) is a good reference to most of the phase points not included in table 2(*a*); the corresponding scaling factors are shown in table 2(*b*). A detailed analysis of this is made in § 6. On the other hand, table 1 refers to a number of phase points not included in tables 2: $P_1$, $P_8$ and $P_{14}$ on the coexistence line, where the system reaches equilibrium too quickly to allow a detailed study of kinetics; and $P_9$, $P_{10}$, $P_{15}$ and $P_{21}$ where the system presents a very slow, untypical evolution probably corresponding to some sort of metastability.

## 6. Power laws

Previous studies (Binder *et al* 1979, Lebowitz *et al* 1983) have introduced the use of simple power laws when analysing the temporal evolution after quenching of the structure function and cluster distributions. Concerning the excess energy, the classical theory of Lifshitz and Slyozov (1961) based on a monoatomic diffusion mechanism is consistent with a power-law behaviour

$$\Delta U \equiv U_t - U_\infty \propto t^{-b} \tag{10}$$

with $b = \frac{1}{3}$. Also, Binder and Stauffer (1974) have shown than an effective cluster diffusion would imply (10) with smaller exponent, say $b = \frac{1}{8}$ at low enough temperatures.

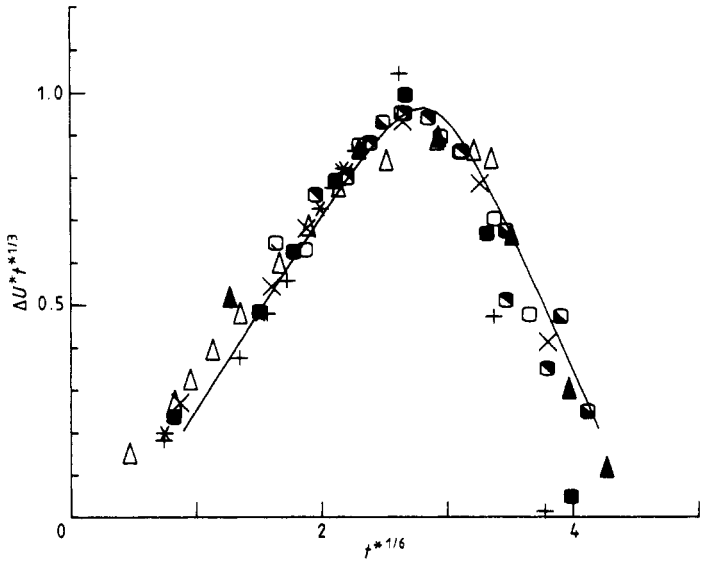


**Figure 4.** $\Delta U^*(t^*)^{1/3}$ is plotted versus $(t^*)^{1/6}$ for the case of shallow quenches: $P_2(+)$, $P_3(*)$, $P_4(\bullet)$, $P_5(\times)$. $P_{11}(\bullet)$, $P_{12}(\blacktriangle)$, $P_{16}(\triangle)$, $P_{17}(\bigcirc)$, $P_{18}(\bullet)$. The full curve is a fit to the data.

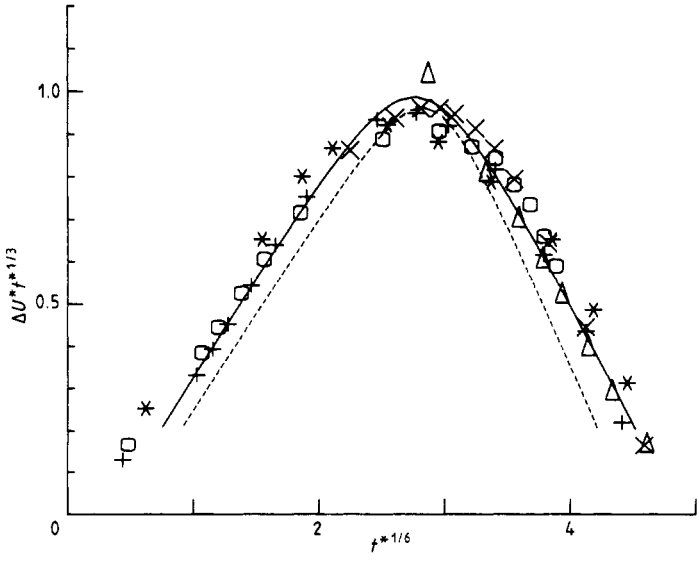


**Figure 5.** As figure 5 but for the case of deep quenches: $P_6(+)$, $P_7(*)$, $P_{13}(\bigcirc)$, $P_{19}(\times)$, $P_{20}(\triangle)$. The full curve is a fit to the data. The broken curve is the same as the full curve in figure 4 and it is included for comparison.

However, the log–log plot in figure 2 clearly shows that there is no time regime that can be described by (10) with a constant value for the exponent $b$. As, however, the simple microscopic mechanisms just mentioned should be relevant during the temporal evolution of the system, we have analysed the data on the assumption that

$$\Delta U^* = \gamma_1 (t^*)^{-1/3} + \gamma_2 (t^*)^{-1/6}. \tag{11}$$

The result is shown in figure 4 where $\Delta U^* (t^*)^{1/3}$ is plotted versus $(t^*)^{1/6}$ for the case of the experiments at $P_6$, $P_7$, $P_{13}$, $P_{19}$ and $P_{20}$ corresponding to *deep quenches*. Figure 5 is a similar plot for the case of the data associated with *shallow quenches*, namely $P_2$, $P_3$, $P_4$, $P_5$, $P_{11}$, $P_{12}$, $P_{16}$, $P_{17}$ and $P_{18}$.

The information provided by figures 4 and 5 seems quite interesting and varied. Firstly, it clearly shows how the excess energy presents a simple scaling with density and temperature. This is similar (but somewhat more general: the situation here holds at any time) to the result in a recent analysis of the behaviour of the structure function in computer simulations (Marro and Vallés 1983). Those figures also seem to confirm the observation (Lebowitz *et al* 1982) that there is a real difference, however small, between the behaviour near $T_c$ or near the coexistence curve for small $\rho$ (the so-called *shallow quenches*) and the one at the centre of the phase diagram for large $\rho$ and low $T$ (*deep quenches*). The data in both cases can be fitted by parabolae or hyperbolae with the axis slightly rotated from the vertical direction.

Figures 4 and 5 also differentiate two (very) well defined regimes during the evolution of the system, in the cases of both deep and shallow quenches. The initial regime is characterised by equation (11) with $\gamma_1 \lesssim 0$ and $\gamma_2 > |\gamma_1|$, thus indicating that the $t^{-1/6}$-law (effective cluster diffusion) is then rather dominant. During the final regime, on the contrary, $\gamma_2 < 0$ and $\gamma_1 > |\gamma_2|$ corresponding to the dominance of the $t^{-1/3}$-law (monoatomic diffusion). The crossover between the two regimes occurs rather sharply around $t^* = 150 \pm 20$, the error indicating the boundaries of the transition region.

## 7. Conclusions

We have described, analysed and compared the data obtained from a series of computer simulations and from some microcalorimetric experiments. Our results strengthen previous findings (Lebowitz *et al* 1983 and references therein) and also seem to suggest some new interesting facts.

The similarity between real and computer generated data is remarkable. In fact, we have shown that, concerning the behaviour of the excess energy versus time, one may group all the phase points considered into two groups, deep and shallow quenches, independently of the system considered: the differences between the behaviours in these two groups (see figure 5), albeit numerically small, are significantly larger than the experimental scatter within each group. This confirms previous results concerning the structure function and cluster distribution.

More precisely, we find that

$$U_t - U_\infty = \alpha_1^{-1} F(\alpha_2 t) \tag{12}$$

where $\alpha_1$ and $\alpha_2$ are scale factors and $F(x)$ is a function (which can be approximated by a combination of simple power laws) that differs slightly according to whether the data refer to deep or shallow quenches (but is otherwise independent of temperature and density). A detailed derivation of equation (12) will be given elsewhere (Toral and

**Table 3.** Values of the parameters in equation (11) characterising the four situations described in the text.

| | Deep quenches | Shallow quenches |
|---|---|---|
| Initial regime | $\gamma_1 = -0.05 \pm 0.01$ | $\gamma_1 = -0.055 \pm 0.005$ |
| | $\gamma_2 = 0.42 \pm 0.02$ | $\gamma_2 = 0.38 \pm 0.01$ |
| Final regime | $\gamma_1 = 2.6 \pm 0.1$ | $\gamma_1 = 3.1 \pm 0.4$ |
| | $\gamma_2 = -0.52 \pm 0.02$ | $\gamma_2 = -0.7 \pm 0.1$ |

Marro 1984). We also provide theoretical estimates for $U_\infty$ in the case of the three-dimensional binary alloy or Ising model; these estimates are fully consistent with the numerical values obtained from the simulations at low densities (where the model system can reach the equilibrium state).

The temporal evolution of the system, in the cases of both deep and shallow quenches, can clearly be characterised by two different regimes. We conclude that each regime may be interpreted as the result of competition between the Lifshitz–Slyozov monoatomic diffusion and the Binder–Stauffer effective diffusion and coagulation of clusters. The latter mechanism happens to be rather dominant during the initial regime, while the system shows afterwards a rather sharp transition to a regime where monatomic diffusion is predominant. More data would be necessary before one could make conclusions (e.g. from a table such as table 3) about significant differences between deep and shallow quenches.

Finally, we should emphasise that the temporal evolution of the excess energy is only described by a combination such as (11) and not by individual power laws $t^{-b}$; that is, it seems inadequate to produce the usual log–log plots looking for single exponents $b$ characteristic of the whole (or part of the) temporal evolution. The same statement probably holds for other quantities such as the moments of the structure function or cluster distributions, mean grain size, etc.

## References


Baker J A 1963 *Phys. Rev.* **129** 99

Binder K 1972 *Physica* **62** 508

Binder K, Kalos M, Lebowitz J and Marro J 1979 *Adv. Colloid Interface Sci.* **10** 173–214

Binder K and Stauffer D 1974 *Phys. Rev. Lett.* **33** 1006

Essam J W and Fisher M E 1963 *J. Chem. Phys.* **38** 802

Goldburg W I 1982 *Scattering Techniques Applied to Supramolecular and Nonequilibrium Systems* ed. S Chen, B Chu and R Nossal (New York: Plenum) pp 383–409

Fratzl P, Lebowitz J, Marro J and Kalos M 1983 *Acta Metall.* **31** 1849–60

Leamy H, Gilmer G and Jackson K 1973 *Phys. Rev. Lett.* **30** 601

Lebowitz J, Marro J and Kalos M 1982 *Acta Metall.* **30** 297–310

—— 1983 *Comm. Solid State Phys.* **10** 201

Lifshitz I M and Slyozov V V 1961 *J. Phys. Chem. Solids* **19** 35

Marro J, Bortz A, Kalos M and Lebowitz J 1975 *Phys. Rev.* B **12** 2000–11

Marro J and Toral R 1983 *Physica* A **122** 563–86

Marro J and Vallés J L 1983 *Phys. Lett.* **95A** 443–6

Murray J L 1983 *Bull. Alloy Phase Diagrams* **4** 55

Penrose O, Lebowitz J, Marro J, Kalos J and Tobochnik J 1984 *J. Stat. Phys.* **34** 399–426

Schwahn D and Schwatz W 1978 *Acta Metall.* **26** 1571

Toral R and Marro J 1984 *Phys. Rev. Lett.* to be published